Numerical study of Kelvin cells for the design of periodic lattice metamaterials

L. Kleine-Wächter [1,2]**, R. Rumpler** [2,3]**, H. Mao** [2,3]**, G. Müller** [1]
[1] Technical University of Munich, Department of Civil and Environmental Engineering,
Arcisstr. 21, D-80333, Munich, Germany
e-mail: **lukas.kleinewaechter@tum.de**

[2] KTH Royal Institute of Technology, MWL Laboratory for Sound and Vibration Research,
Teknikringen 8, SE-100 44 Stockholm, Sweden

[3] KTH Royal Institute of Technology, The Centre for ECO2 Vehicle Design,
Teknikringen 8, SE-100 44 Stockholm, Sweden

Abstract

Artificially-composed materials, often called metamaterials, are an increasingly considered measure for vibration control. By carefully arranging the material micro-structure, significant vibration attenuation is achievable in targeted frequency bands from resonant and wave scattering effects. An approach in designing materials for vibration control are micro-structures assembled from periodic cellular lattices. Such architectures result from the spatial repetition of cellular units that can be dynamically tuned by controlling the lattice characteristics. This contribution investigates the prospects of a three-dimensional lattice structure for application in vibration control. A unit cell design strategy is proposed based on the isometric Kelvin cell. By imposing twists on the faces of the Kelvin cell, a potential tuning mechanism for the cell's dispersive properties is introduced. Selected unit cell designs obtained from this approach are investigated in terms of the dispersion characteristics of 1D-infinite structures.

1 Introduction

Metamaterial is a collective term for a class of materials, which are characterized above all by one thing: Not the actual material, but some of its properties are "*meta*", i.e. going beyond the usual [1]. Artificially generated material microstructures give rise to effective properties on the macro-level that cannot be achieved by the material which is constituting the microstructure [2]. Lattice materials are a vivid branch in the wide-ranging research field of metamaterials [3]. Their microstructure is typically composed of cellular units of interlaced trusses that are periodically repeated in space. The formation of truss-based networks offers vast design capabilities to attain unusual properties on the macroscopic level. In mechanics and acoustics, vanishing shear stiffness at a finite bulk modulus [4], negative Poisson ratio (auxetics) [5], and frequency band gaps [6] are a few examples of "meta-behavior" obtained from architected lattices, among others.

The ability to generate tunable band gaps makes lattice materials particularly attractive for vibroacoustic applications. Band gaps are regions in the wavenumber-frequency spectrum where the free wave propagation is inhibited. In practice, materials exhibiting band-gap characteristics are capable of significant vibration attenuation performance when subjected to vibrations in the concerning band gap frequency ranges [7]. In that sense, periodic lattices serve multi-functional purposes: While providing static stiffness and load-bearing capacities, they simultaneously act as frequency filters [8]. In case the wavelength of propagating waves matches the lattice dimensions, waves scattered by the lattice interfere destructively, leading to so-called BRAGG-scattering band gaps [9]. Owing to the dependency of this mechanism on the lattice dimensions, achieving band gaps in the low-frequent regime is complicated as large periodicity constants are required. A

solution to create band gaps far below the BRAGG scattering limit are embedded structural units for resonant behavior. The structural units are designed to resonate out-of-phase to the motion of the host structure [6]. Resulting band gaps do not depend on the lattice dimensions but are dictated by ratios of mass and stiffness. Thus, the dimensions of resonant units may be smaller than the wavelength of affected waves, which can be exploited to create compact designs with substantial band gap performance [10]. Several studies have shown that adding point-like masses to a host lattice facilitates significant band gaps in the low-frequent range while maintaining sufficient static properties [11, 12, 13]. Yet, when targeting resonant band gaps to very low frequencies, the required mass addition may be severe. Therefore, other concepts seek to create band gaps by exploiting the inherent resonances of the constitutive lattice to generate band gaps in both low- and high-frequent frequency regimes [14, 15].

Another direction in molding the lattice topology to generate band gaps are chiral lattices. *Chirality* classifies an object as not being superimposable with its mirror image by pure translations or rotations [16]. Cellular lattice units subject to chirality can, among other effects, enforce coupling of rotational and translational deformation, such that an additional inertia factor enters the dynamic of the chiral lattice [17]. By amplifying this inertia term using well-defined mass elements, significant band gaps in the low-frequent regime are attainable with a minimal mass penalty [18, 19, 20]. Several lattice structures involving chirality as a design paradigm for bandgap performance have been proposed for 2D and 3D cases [21, 22]. However, chiral effects are often only available in a specific direction, which limits the possibilities of connecting chiral unit cells and requires a targeted directive excitation of the lattice to unleash chiral effects. To overcome this limitation, ongoing research works seek to embed chiral effects in multiple directions [23, 24].

This contribution discusses the potential of a unit cell design approach to achieve tunable performance of the lattice's dispersive properties. The initial lattice is derived from an isometric Kelvin cell model. This unit cell features six square-shaped faces which are the key elements of the proposed tuning approach. By independently twisting the square faces, altered unit cell designs are generated, which are topologically equivalent to the isometric reference cell. In particular, the lattice design approach allows to establish chirality in three principal directions while maintaining the simple-cubic structure. In a comparative study, the dispersion relation of 1D infinite lattices obtained from twisted unit cells is discussed. It is shown that the band structure can be significantly influenced by the imposed levels of twisting, such that band gaps and chiral coupling effects are inducible. The research presented builds upon initial contributions by some of the co-authors [25, 26].

2 Metamaterial design & modelling approach

2.1 Kelvin cell and twisting approach

The metamaterial design ansatz is deduced from a Kelvin cell (KC), also denoted as *truncated octahedron* or *tetrakaidecahedron* as shown in Fig. 1. The unit cell features six identical square and eight hexagonal faces formed by a network of 36 ligaments. Each of the 24 vertices rigidly connects the ends of coinciding ligaments. The cell exhibits isometry with a characteristic length h_c and cubic material symmetry.

The KC structure serves as foundation block for a cellular truss-based microstructure. In the following, the idea of *twisting* the KC structure as proposed by the authors of Ref. [26] is considered, as a key factor to investigate an additional tuning mechanism of underlying cell dynamics. Geometrical modifications imposed to the reference geometry are achieved through coordinate transformations that describe pairwise in-plane rigid body rotations of the cell's square faces. The rotational angles applied to opposite square faces are equal in absolute value, but can either be symmetric or anti-symmetric, meaning clockwise or counter-clockwise rotation of opposing faces. The latter case establishes chirality with respect to each middle plane parallel to the pairs of twisted faces. In both cases, it is presumed that the squares are undeformed after rotation, and all vertices remain connected through the same ligaments with altered lengths compared to the isometric reference geometry. Thus, a modified structure is topologically equivalent to the isometric Kelvin cell and all twisted faces remain in their original planes, meaning that generated lattice architectures retain a simple-cubic nature.
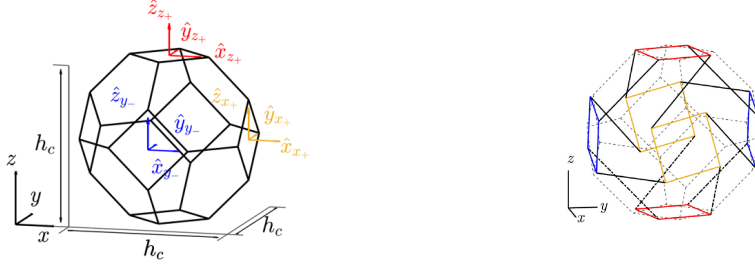
Figure 1: Isometric Kelvin cell reference and coordinate definitions (left) and geometry after twisting all six square faces (right) [26].

Mathematically, the *twisting*-approach is expressed by transformations between the cell's local and global coordinate systems using Euler rotation angles $[\theta_j^{\hat{x}}, \theta_j^{\hat{y}}, \theta_j^{\hat{z}}]$. The sets of local coordinates $(\hat{x}, \hat{y}, \hat{z})_j$ originate at the center of the respective square faces denoted j and are parallel to the isometric cell's global coordinates (x, y, z) as shown in Fig. 1. Assuming successive, independent rotations around the axes $\hat{z}$, $\hat{y}$ and $\hat{x}$, the rotation matrices read

$$[R]_j = \begin{bmatrix} 1 & 0 & 0 \\ 0 & \text{c.}\theta_j^{\hat{x}} & \pm\text{s.}\theta_j^{\hat{x}} \\ 0 & \text{s.}\theta_j^{\hat{x}} & \text{c.}\theta_j^{\hat{x}} \end{bmatrix} \begin{bmatrix} \text{c.}\theta_j^{\hat{y}} & 0 & \text{s.}\theta_j^{\hat{y}} \\ 0 & 1 & 0 \\ \pm\text{s.}\theta_j^{\hat{y}} & 0 & \text{c.}\theta_j^{\hat{y}} \end{bmatrix} \begin{bmatrix} \text{c.}\theta_j^{\hat{z}} & \pm\text{s.}\theta_j^{\hat{z}} & 0 \\ \text{s.}\theta_j^{\hat{z}} & \text{c.}\theta_j^{\hat{z}} & 0 \\ 0 & 1 & 0 \end{bmatrix} \tag{1}$$

with $\text{c.}\cdot = \cos(\cdot)$ and $\text{s.}\cdot = \sin(\cdot)$. Consequently, the location of points $(\hat{x}, \hat{y}, \hat{z})_j^T$ at the square face j of the KC reference lattice is given by

$$\left(\hat{x}', \hat{y}', \hat{z}'\right)_j^T = [R]_j \left(\hat{x}, \hat{y}, \hat{z}\right)_j^T \tag{2}$$

after twisting the isometric structure. Fig. 2 gives examples of the isometric and twisted cells. The concept of twisting is expected to add another variable to the unit cell design, allowing for the parametric design of cell architectures with substantially differing dynamic properties but with identical material and lattice settings and the same topology.

(a) Isometric reference   (b) One-axial twist (achiral)   (c) One-axial twist (chiral)   (d) Three-axial twist (chiral)
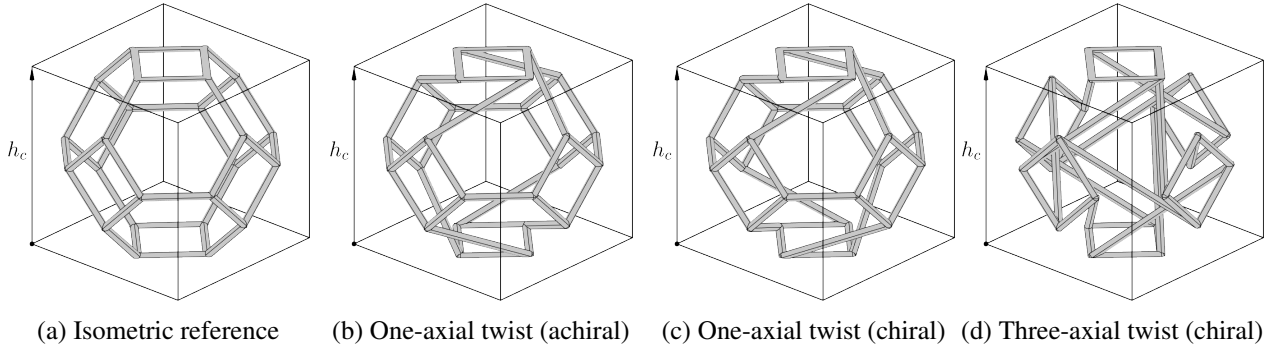
Figure 2: Illustrations of elementary cells obtained from the *twisting*-approach according to equation (1). In examples (b) to (d), the twist angle has been adjusted to $\theta_j^{\hat{i}} = 90°$ where j denotes the twist axes and $\hat{i}$ the local square face coordinates (compare Fig. 1). Cases (b) and (c) are obtained from symmetric and anti-symmetric rotations of opposing faces, respectively. Note that the upper and lower square faces are only half within the elementary cell to facilitate 1D-periodicity in the corresponding direction.
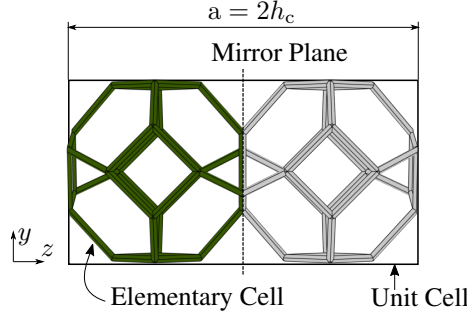
Figure 3: Example of the unit cell composition for 1D translational periodicity in z-direction. Mirroring the twisted elementary cell (shaded in green) with respect to the cell border yields the unit cell with coinciding faces.

2.2 Unit cell composition for 1D-periodicity

While the isometric Kelvin cell may serve as a unit cell to map the periodicity of both one, two- and three-dimensional periodic lattices, the twisting approach according to equation (1) affects the cellular symmetry and, thus, the choice of translational periodicity. In the case of configurations deduced from anti-symmetric rotations, the induced chirality is by definition associated with a miss-match of opposing square faces, meaning that corresponding faces are not superimposable when projected on their parallel planes. As a result, pure translations of a twisted chiral building block would lead to an incompatible arrangement due to non-overlapping square faces at the junction of adjacent cells. Exceptions are chiral configurations twisted by multiples of $45°$-angles that author coinciding faces independent of the cell's chiral character. On the contrary, achiral cells generated by symmetric rotations are exempted from this effect as the cell symmetry is maintained and square faces remain superimposable for all feasible twist angles without exceptions.

To address these implications of twisted chiral cells, all cellular lattices discussed in this contribution are constructed from unit cells composed of two elementary twisted Kelvin cells related to each other through a mirror operation. A twisted elementary cell is mirrored with respect to a plane containing one of the opposing square faces, generating a double-cell with coinciding faces and nodes at its junctions. The geometry resulting from this operation defines a unit cell setting up a lattice with one-dimensional translational periodicity and a lattice constant resembling twice the length of an elementary cell. In the case of untwisted isometric or twisted achiral elementary cells, the mirror operation yields the same result as if the elementary unit was translated on itself by one unit length. The effects of this choice of unit cell outline in terms of wave dispersion are discussed in Sec. 3.2. Fig. 3 gives an example of a unit cell assembled from the described procedure. If the periodicity shall be extended to two or three dimensions, the described procedure can be analogously employed to form unit cells of four and eight elementary building blocks, respectively.

2.3 Numerical Setup

The band structures representing the dispersion properties are computed through the Finite Element method and BLOCH-FLOQUET theory to connect the displacements of the unit cell boundaries. The considered periodicity formulation is readily available in the commercial software COMSOL MULTIPHYSICS which was used to implement the numerical models and solve the following equations. For one-dimensional periodicity, the displacements of nodes of opposing bottom and top square faces are spatially constrained by

$$\boldsymbol{u}_{\text{bottom}} = \boldsymbol{u}_{\text{top}} e^{-ik a}, \tag{3}$$

where $k \equiv k_z$ is the wavenumber and a the lattice constant. All other boundaries are considered as traction-free. Under the assumption of absence of external forces and damping, the eigenvalue problem

$$\left[\mathbf{K} - \omega^2 \mathbf{M} \right] \boldsymbol{u} = 0 \tag{4}$$

in terms of the circular eigenfrequency $\omega = \omega\left(k\right)$ and the unit cell's global mass and stiffness matrices $\mathbf{K}$ and $\mathbf{M}$ can be derived, representing the free wave motion. The eigenvalue problem is solved for each pair $\omega\left(k\right)$ by sweeping the wavenumber k_z along the irreducible part of the first BRILLOUIN zone $k_z \in [0, \pi/\mathrm{a}]$, where $\mathrm{a} = 2h_c$ is the lattice constant for the given definition of unit cells. Linear-elastic material behavior is assumed, and for the entire domain epoxy is chosen as constitutive material which is commonly available in additive manufacturing procedures. Table 1 lists the material and geometrical parameters applied for all calculations.

The choice of unit cell comprising 68 trusses in total naturally leads to a densely stacked band structure with multiple occurrences of crossing bands, aggravating an intuitive interpretation of the dispersion diagram. To simplify the band structure and allow for a fast attribution of wave motions to the dispersion branches, the band structures are investigated considering a mode polarization factor as suggested by the authors of Ref. [27] and [28]. To distinguish between the in- and out-of-plane motion of modes shapes corresponding to each solution of the eigenvalue problem, the polarization factor

$$p = \frac{\int_V |u_z|^2 \mathrm{d}V}{\int_V \left(|u_x|^2 + |u_y|^2 + |u_z|^2\right) \mathrm{d}V} \tag{5}$$

is computed for each mode from the displacements in x, y and z-direction, where V is the volume of the entire unit cell. The dispersion branches are colored according to eq. (5) such that values from 0 (blue) to 1 (red) mark a change from a pure in-plane (x, y) to a pure out-of-plane (z) mode deformation characteristic.

3 Twisting the Kelvin cell: Parametric study

3.1 Increasing angles of twist

At first, the impact of increasing twist angles on the dispersion relation of lattices with one-dimensional translational periodicity is investigated. To this end, varying twist angles $\theta_{z\pm}^{\hat{z}}$ with respect to the global $\hat{z}$-axis are imposed, which coincides with the direction of periodicity. Associated square faces are rotated symmetric and anti-symmetric. Therefore, each elementary building block exhibits chirality with respect to its middle plane. The unit cells are obtained from mirror operations, as reported in Sec. 2.2, and shown in Fig. 5. By twisting only the z_+- and z_- square faces, it is made sure that the applied geometrical changes are kept small with respect to the isometric reference, which serves as a basis of comparison. Fig. 5 reports the dispersion relation of a selection of tested structures from small to large twist angles, with $120°$ being defined as the maximum angle as larger values reach the limits of manufacturing.

Focussing on the similarities first, all structures exhibit wave propagation characteristics similar to an equivalent homogeneous material in the lower-frequent regime, carrying waves with a non-dispersive longitudinal, two transverse, and, additionally, a torsional polarization. For higher frequencies, the wave propagation is fully dispersive, and associated mode shapes are governed by the interplay of individual deformations within the trusses of the unit cell. As can be seen, adjacent branches of identical polarization fold at the corner $k = \pi/\mathrm{a}$ of the irreducible BRILLOUIN-zone and are seemingly reflected. By comparing the mode shapes of connected branches in the lower-frequent regime, exemplarily shown in Fig. 6 for longitudinal and torsional polarization, one can observe that the unit cell's elementary blocks oscillate in-phase for increasing wavenumbers and change to an out-of-phase motion after being deflected at the edge of the BRILLOUIN zone. This pattern is consistent with the dispersive behavior of an infinite mass-spring chain having regular mass and stiffness

Table 1: Material and geometry properties used in the FE calculations of all lattice structures.

Material (epoxy)		Geometry	
Density $\left[\mathrm{kg/m^3}\right]$	1180	Elementary cell height h_c [mm]	50
YOUNG'S modulus [GPa]	4.35	Characteristic length a [mm]	100
Shear modulus [GPa]	1.59	Truss cross-section radius R [mm]	1.0

(a) Isometric reference   (b) $\theta_{z\pm}^{\hat{z}} = \pm45°$ (c) $\theta_{z\pm}^{\hat{z}} = \pm90°$ (d) $\theta_{z\pm}^{\hat{z}} = \pm120°$
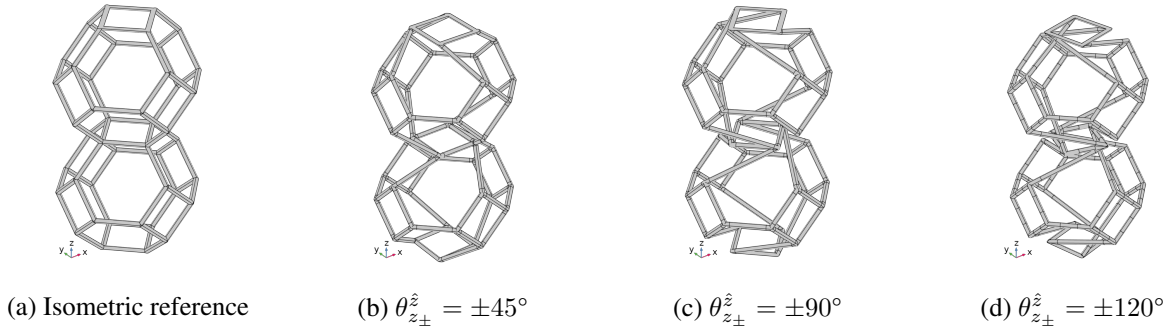
Figure 4: Unit cells obtained from the isometric Kelvin cell (a) and from increasing twist angles $\theta_{z\pm}^{\hat{z}}$ ((b)–(d)).

(a) Isometric reference   (b) $\theta_{z\pm}^{\hat{z}} = \pm45°$ (c) $\theta_{z\pm}^{\hat{z}} = \pm90°$ (d) $\theta_{z\pm}^{\hat{z}} = \pm120°$
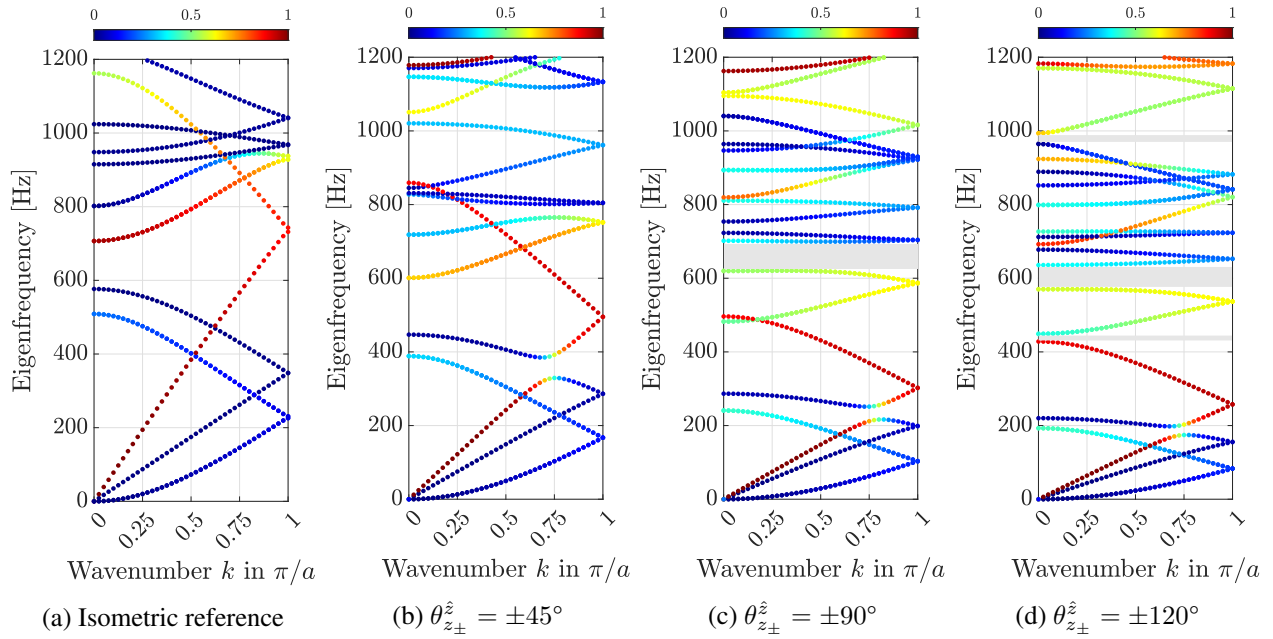
Figure 5: Dispersion relation in the irreducible BRILLOUIN zone for increasing angles of twist. All unit cells have been twisted anti-symmetric according to Eq. (1), thus exhibiting chirality in their elementary building blocks. Colors indicate the polarization of modes from in-plane (blue) to out-of-plane (red). Grey regions highlight full band gaps.

attributes, so-called *monoatomic* chains as reported in Ref. [29]. The modal behavior of such mass-spring chains is characterized by a low-frequent *acoustical* branch, where the chain members oscillate in-phase, and a high-frequent *optical* branch, displaying an out-of-phase motion of adjacent chain members [29]. Given these qualitative similarities, the lower-frequent dispersion of infinite Kelvin cell architectures may be explained from analogies to mass-spring chains; with the mass being determined by the weight of the trusses, whereas the stiffness is not solely dictated by material, but also by the connection pattern of trusses. This analogy is exploited in Sec. 3.3 to break the connection of acoustical and optical branches.

The results presented in Fig. 5 further suggest that increasing twist angles are accompanied by a decrease of the unit cell's eigenfrequencies, evoking a collective, but nonuniform downward-tuning of all branches in the frequency range of interest. The reduction is particularly noticeable when comparing the slopes of the red out-of-plane branches, denoting a longitudinal wave polarization. I. e., at the edge of the BRILLOUIN zone $k = \pi/a$, the eigenfrequency of the isometric structure (Fig. 5a) reduces from 731 Hz to 275 Hz for the unit cell twisted by 120° (Fig. 5d), linked with a decrease of the longitudinal phase speed. This tuning effect is traceable to changes in the cell's stiffness properties as a consequence of twisting. The discussed longitudinal modes vibrate in direction of periodicity, with trusses being oriented axially in z-direction carrying a large amount of the stiffness of the mode. As the twist angle increases, trusses being connected to twisted faces

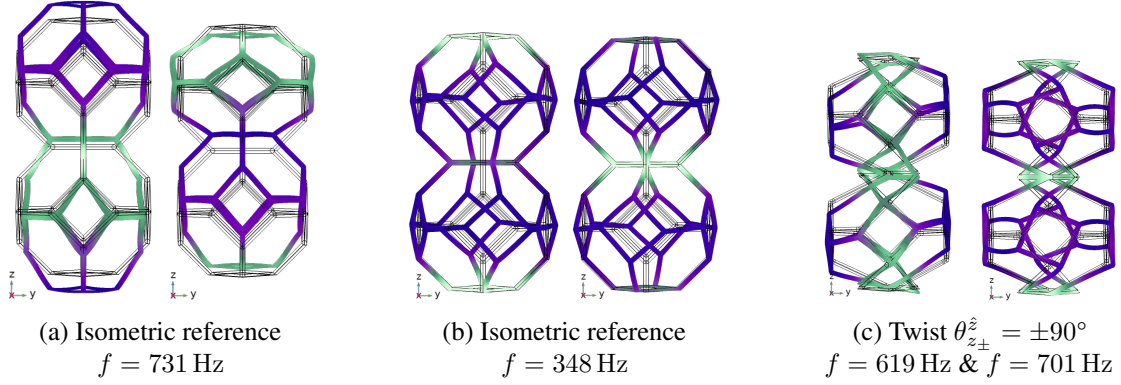|		
(a) Isometric reference $f = 731\,\text{Hz}$	(b) Isometric reference $f = 348\,\text{Hz}$	(c) Twist $\theta^{\hat{z}}_{z\pm} = \pm 90°$ $f = 619\,\text{Hz}\ \&\ f = 701\,\text{Hz}$

Figure 6: Mode shapes of selected unit cells: (a) and (b) display the in- and out-of phase motion of the longitudinal and torsional wave as the branches fold at $k = \pi/\text{a}$. (c) shows the band gap edge modes at $k = 0$.

elongate and change their orientation in the lattice, such that the portion of axial loading is reduced, while bending deformations come to the fore. As beams deform more easily in bending than in axial loading, the overall axial stiffness of the mode reduces, leading to the observed changes in the eigenfrequencies and correspondingly the slope. Accordingly, modes having flexural and torsional polarization are less affected by the change of axial stiffness which results in a separation of dispersion bands having different polarizations. Fig. 5a gives an example for this effect: Here, branches of longitudinal, flexural and torsional polarization cross at $930\,\text{Hz}$ for a wavenumber of $k = 0.7\pi/\text{a}$. As the twist angle increases to $90°$ in Fig. 5c, the crossing of branches unravels, and corresponding values of the longitudinal and torsional branches drop down to respectively $382\,\text{Hz}$ and $700\,\text{Hz}$ at $k = 0.7\pi/\text{a}$, while the flexural band reduces to $610\,\text{Hz}$ and notably flattens. As a consequence of this twisting-induced band separation, a full band gap opens in the range of $620\,\text{Hz} - 700\,\text{Hz}$. When the twist angle is further adjusted to $120°$ in Fig. 5d, the center frequency of this band gap decreases, as well as the band width which spans from $570\,\text{Hz}$ to $635\,\text{Hz}$. For this value of twist, one can also observe the occurrence of another low-frequent band gap ($431\,\text{Hz}$ to $450\,\text{Hz}$) and a high-frequent one ($965\,\text{Hz}$ to $993\,\text{Hz}$).

As a general result, the study indicates that the twisting approach may provide a tuning method for the Kelvin cell's dispersion characteristics, governed by changes of the stiffness characteristics of modes as the twist angle is varied. The results confirm that full band gaps which are absent in the isometric design can be induced and tuned. Twist angles in the intermediate range of discussed ones were also taken into account, presenting qualitatively similar outcomes. Apart from the band separation effect, investigating the dispersion relations reveals another interesting effect associated with the unit cell's chirality: As can be seen from Fig. 5b to Fig. 5d, the 4th and 5th branches representing respectively a longitudinal and torsional wave motion do not cross, unlike the isometric unit cell. Instead, the branches seemingly separate and thus, feature a small gap. This effect is subject to the subsequent investigation.

3.2 Chiral & achiral unit cells

The previous study solely focused on unit cells assembled from chiral elementary cells. As a next step, the dispersive behavior of unit cells configured from chiral and achiral elementary cells is compared for a fixed twist. The twist angle is set to $45°$, implying that faces coincide independent of symmetric or anti-symmetric rotations. Consequently, this allows for special configurations of the unit cell apart from the mirroring approach introduced in Sec. 2.2. Inspired by the work of Bergamini *et al.* [19] on using elements of opposite chirality as a design paradigm of phononic crystals with band gap performance, three configurations are devised: In Fig. 7b and Fig. 7c, the same chiral elementary cell is used, but once mirrored and once translated to obtain the unit cell. In contrast, the unit cell depicted in Fig. 7a is configured by an achiral elementary cell, such that both translating and mirroring yield the same unit cell outline. Fig. 8 compares the dispersion relation of all unit cells with respect to the isometric arrangement. Comparing the isometric and achiral arrangement, one notices qualitative agreement in the progression of the first dispersion branches up to $600\,\text{Hz}$,

(a) Achiral
$\theta_{z_\pm}^{\hat{z}} = 45°$

(b) Chiral – mirrored
$\theta_{z_\pm}^{\hat{z}} = \pm 45°$

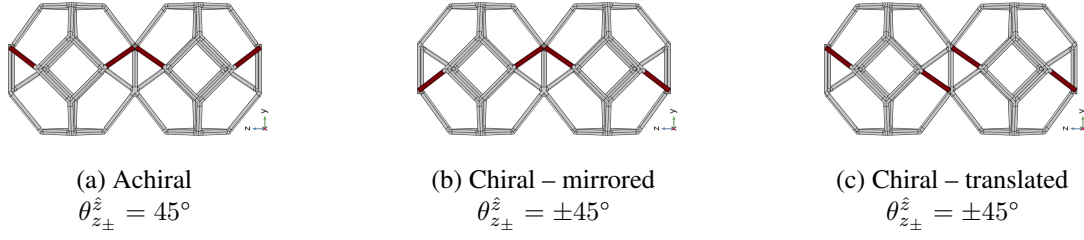(c) Chiral – translated
$\theta_{z_\pm}^{\hat{z}} = \pm 45°$

Figure 7: Unit cell configurations in (z, y)-view, showing the fully twisted. Twist angles and geometric properties refer to elementary cells; mirroring or translation describes the operation to configure the unit cell for chiral setups. Trusses in the front are shaded in red to highlight the geometrical differences.

resembling mass-spring chain-like behavior. The twisted achiral structure is subjected to twisting-induced down-tuning and flattening of branches as described in the previous section, opening a full band gap from 839 Hz to 914 Hz. Unit cells obtained from mirroring a chiral elementary cell do not possess a complete band gap as revealed in Fig. 8c and 8d. Yet, in contrast to the isometric and achiral cell, another effect arises concerning its 3rd and 5th band, representing longitudinal and torsional wave motion. A partial band opens between these branches, ranging from 329 Hz to 384 Hz (Fig. 8c). This observation can be attributed to the elementary cell's chirality, which introduces compression-torsion motion coupling of associated mode shapes. Fig. 9 compares the mode shapes at the gap edge located at $k = 0.75\pi/a$. For both, an overall compression-torsion coupled deformation is observable, owing to bending deformations of the twisted structural parts being converted to rotational movements of connected square faces and vice versa. The coupling effect is also indicated by the polarization factor which switches to similar values as the branches approach. The polarization of both bands again changes to the initial in-and out-of-plane characteristic as the wavenumber increases, which suggests that compression-torsion coupling only emerges for specific, matching solutions in the wavenumber-frequency domain. The same effect is observable in Fig. 8d for the chiral translated case

(a) Isometric reference

(b) $\theta_{z_\pm}^{\hat{z}} = \pm 45°$
(achiral)

(c) $\theta_{z_\pm}^{\hat{z}} = \pm 45°$
(chiral – mirrored)

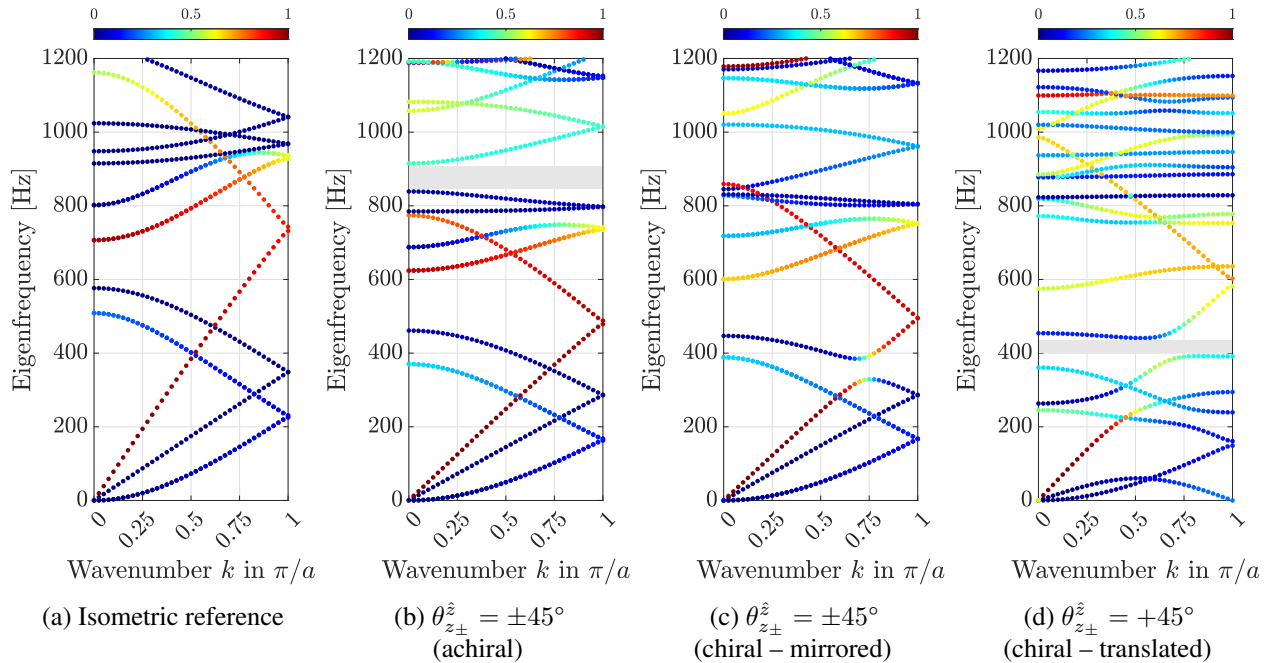(d) $\theta_{z_\pm}^{\hat{z}} = +45°$
(chiral – translated)

Figure 8: Dispersion relation in the irreducible BRILLOUIN zone for unit cells of equal twist, but varying symmetry characteristics. The terms *translated* and *mirrored* refer to the operation applied to elementary cells to form the unit cell as shown in Fig. 7. Chirality and achirality apply with respect to elementary cells. Colors indicate the polarization of modes from in-plane (blue) to out-of-plane (red). Grey regions highlight full band gaps.

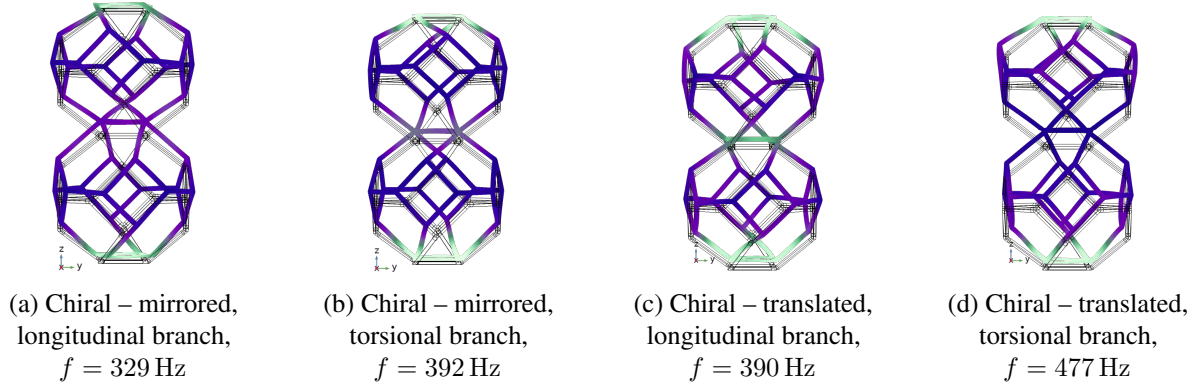| (a) Chiral – mirrored, | (b) Chiral – mirrored, | (c) Chiral – translated, | (d) Chiral – translated, |
| longitudinal branch, | torsional branch, | longitudinal branch, | torsional branch, |
| $f = 329\,\mathrm{Hz}$ | $f = 392\,\mathrm{Hz}$ | $f = 390\,\mathrm{Hz}$ | $f = 477\,\mathrm{Hz}$ |

Figure 9: Compression-torsion coupled mode deformation shapes at the edges of the partial gap between longitudinal and torsional branches of chiral unit cells in Fig. 7b and 7c. All mode shapes correspond to a wavenumber of $k = 0.75\pi/\mathrm{a}$.

around wavenumbers $k = 0.45\pi/\mathrm{a}$ and $k = 0.7\pi/\mathrm{a}$. As the 3$^{\text{rd}}$ longitudinal branch approaches the 5$^{\text{th}}$ and 7$^{\text{th}}$ band having both torsional characteristics, the bands separate, even leading to a full band gap from $390\,\mathrm{Hz}$ to $454\,\mathrm{Hz}$. Fig. 9c and 9d depict the corresponding mode shapes.

Two major differences can be noted when comparing the dispersion relation of both chiral arrangements. First, the spectrum of the chiral–translated unit cell is populated by flat dispersion bands of in-plane polarization starting from $800\,\mathrm{Hz}$. These result from an altered connection pattern at the cell junction compared to the mirrored design, which facilitates the emergence of modes dominated by local deformations of the square faces. Thus, the deformations do not propagate across the cell boundaries to excite a global wave motion. A discussion and examples of this effect are presented in Sec. 3.4.

Second, the translated arrangement exhibits a splitting of the first two transverse bands, unlike the chiral-mirrored unit cell where flexural modes with rotation around the x- and y-axis yield the same eigenvalues. Moreover, one of the split branches in Fig. 8d displays an unusual parabolic shape, which implies a change of sign of the group speed and zero group speed at the maximum located at $k = 0.5\pi/\mathrm{a}$. The splitting of flexural bands can be attributed to the changes in the unit cell's symmetry conditions: The chiral–translated arrangement does not possess any mirror symmetries perpendicular to the direction of the imposed periodicity, which is followed by heterogeneous stiffness conditions for transverse motions around the x- and y-axis. Therefore, doubled eigenvalues reduce and a splitting of associated bands occurs. The occurrence of a parabolic dispersion shape, however, cannot be explained from symmetry conditions. Validating the dispersion relation using a chiral–translated unit cell with a twist of $90°$ led to qualitatively similar results. In Ref. [30], the existence of dispersion curves that are not monotonic, but change the slope within the Brillouin zone is demonstrated using a *beyond nearest neighbor* assumption. Here, a three-fold mass-spring chain is employed, where the dynamic interactions are not restricted to adjacent masses but extend to the second nearest neighbor in the chain by incorporating additional springs. In Ref. [31], dispersive behavior according to *beyond nearest neighbor*-theory is confirmed for a manufacturable 3D chiral unit cell. Thus, chirality in connection with interactions that run beyond adjacent unit cells could provide a tentative explanation approach, however, the source of the observed unusual dispersion behavior is left to conjecture at the momentary stage of this research.

In conclusion, the results reveal that unit cells constructed from chiral twisted elementary cells possess compression-torsion coupled modes and band gaps between branches of longitudinal and torsional polarization. Thus, chiralty obtained from twisting the Kelvin cell may provide another lever to induce to engineer unit cells with band gap properties. Changing the orientation of chiral elements within the unit cell by either mirroring or translation does not facilitate the emergence of band gaps. Composing unit cells from mirroring is the preferred procedure as it is applicable to arbitrary angles of twist.

3.3 Partial twisting

The study discussed in Sec. 3.1 gave indications that the dispersion relation of Kelvin cell-based lattices resembles monoatomic mass-spring chains. Now, the elementary building blocks are modified to generate a structure in resemblance to a diatomic chain featuring altering spring stiffnesses. This is achieved by imposing only partial twists to the isometric Kelvin cell such that the connection pattern between adjacent cells in the infinite arrangement is altered. Unlike the previously discussed structures, twisting is only imposed on a single square face while keeping its opposing face intact, such that $\theta_{z_+}^{\hat{z}} \neq 0$ and $\theta_{z_-}^{\hat{z}} = 0$ and vice versa holds. The unit cell is again assembled by mirroring the elementary cell. Fig. 10 shows a unit cell constructed from partial twisting with $45°$ compared to the "fully" twisted unit cell used in the previous studies. As can be seen, translating the unit cell composes a chain of unit cells with their junctions switching from twisted to untwisted. As a further benefit, the approach is not restricted to specific twist angles, but is available for arbitrary twist angles. Fig. 11 presents the dispersion relation of two unit cells compared to the isometric reference and a fully twisted arrangement.

The dispersion relation resulting from the partially twisted arrangement in Fig. 11c exhibits behavior similar to the targeted diatomic chain concerning the first six branches, with the acoustical and optical branches being apart at the edge of the BRILLOUIN zone, unlike the fully twisted and isometric unit cells. In particular, the longitudinal out-of-plane branches are affected, showing a separation ranging from $507\,\mathrm{Hz}$

(a) Full twist $\theta_{z_\pm}^{\hat{z}} = \pm45°$ (b) Partial twist $\theta_{z_-}^{\hat{z}} = 45°, \theta_{z_+}^{\hat{z}} = 0°$
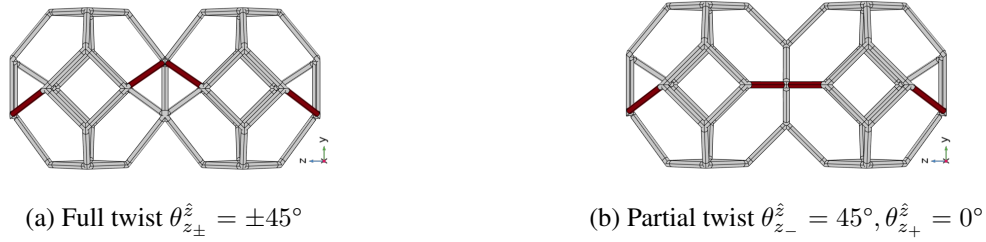
Figure 10: Unit cell configuration in (z, y)-view, showing the fully twisted (a) and partially twisted (b) structures. Trusses in the front are shaded in red to highlight the geometrical differences.

(a) Isometric reference   (b) $\theta_{z_\pm}^{\hat{z}} = \pm45°$ (c) $\theta_{z_-}^{\hat{z}} = 45°, \theta_{z_+}^{\hat{z}} = 0°$ (d) $\theta_{z_-}^{\hat{z}} = 30°, \theta_{z_+}^{\hat{z}} = 0°$
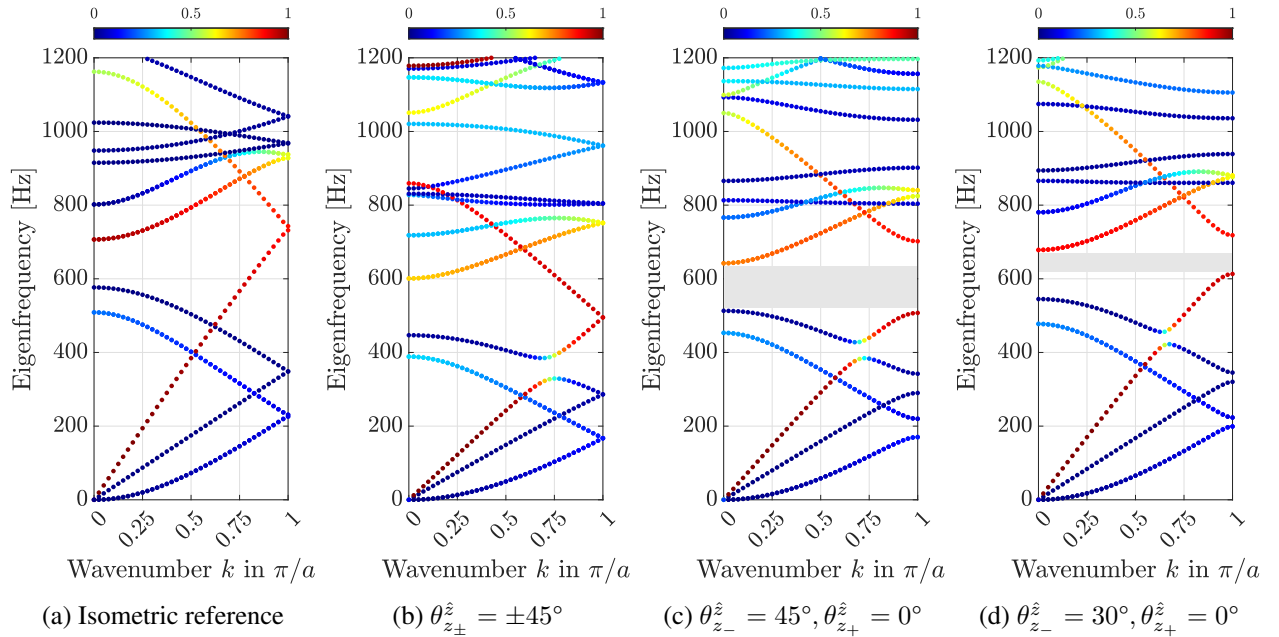
Figure 11: Dispersion relation in the irreducible BRILLOUIN zone for full and partially twisted unit cells as shown in Fig. 10. Chirality and achirality apply with respect to elementary cells. Colors indicate the polarization of modes from in-plane (blue) to out-of-plane (red). Grey regions highlight full band gaps.
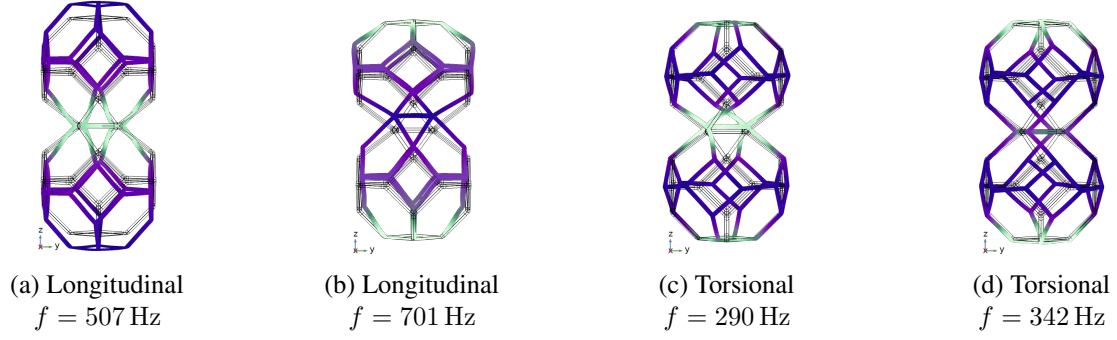
(a) Longitudinal
$f = 507\,\text{Hz}$

(b) Longitudinal
$f = 701\,\text{Hz}$

(c) Torsional
$f = 290\,\text{Hz}$

(d) Torsional
$f = 342\,\text{Hz}$

Figure 12: Frequency gap and phase switch of modes at the edge of the BRILLOUIN zone $k = \pi/a$. All mode shapes correspond to the partially twisted unit cell whose dispersion relation is shown in Fig. 11c.

to 701 Hz at $k = \pi/a$. This gives rise to a significant band gap in the low-frequent regime, ranging from 513 Hz to 642 Hz, which is absent in the isometric and fully-twisted dispersion relation. Corresponding mode shapes of longitudinal and torsional wave motion are shown in Fig. 12. Note that the partially twisted structure still displays a split of the torsional and longitudinal branch around $k = 0.7\pi/a$, resulting from the twisting-induced axial-rotation coupling. The bandgap between the acoustical and optical branch of a diatomic mass-spring chain at the edge of the BRILLOUIN zone is determined by the ratio of spring stiffness and is, therefore, tunable. To demonstrate that this effect holds for the given lattice arrangements, Fig. 11d presents the dispersion relation of a unit cell having a partial twist of only $30°$. Here, the size of the gap induced between the acoustic and optical branches changes significantly, i.e. comprising the range of 613 Hz to 718 Hz for longitudinal polarization, which consequently diminishes the size of the full band gap.

The given examples demonstrate that partial twists of the Kelvin cell are a way to generate low-frequent band gaps, resulting from changing local stiffness characteristics of the cell. In analogy to diatomic mass-spring chains, the gaps can be effectively tuned by the variation of the twist angle, which simultaneously affects the stiffness at the junction of adjacent cells. In the given case, twisting the isometric unit cells only affected the length and direction of 8 out of 68 trusses of the unit cells, leading to significant full band gaps.

3.4 Combining untwisted and twisted cells

As the last example, a unit cell obtained from a combined arrangement of unit cells is studied. While all previous studies feature unit cells composed of elementary cells that are strongly related to each other either by mirroring or twisting, the following structure results from combining the isometric Kelvin cell with a cell being fully twisted by $\pm 90°$ at all square faces. In opposition to the isometric cell, the fully twisted cell does not comprise any mirror symmetries, but chirality with respect to all opposing square faces. Full twisting is applied to form a cell whose stiffness is affected equally along all principal directions, unlike the partially twisted ones presented in Sec. 3.3. The unit cells are presented in Fig. 13. The comparison of the dispersion relation of both arrangements in Fig. 14 reveals drastic changes in the band structure. By combining
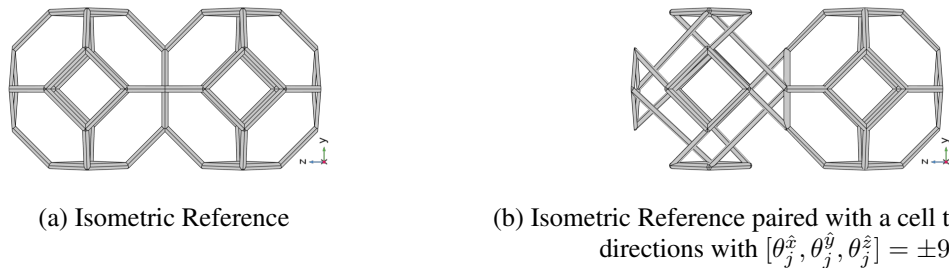

(a) Isometric Reference

(b) Isometric Reference paired with a cell twisted in all directions with $[\theta_j^{\hat{x}}, \theta_j^{\hat{y}}, \theta_j^{\hat{z}}] = \pm 90°$

Figure 13: Unit cell configuration in (z, y)-view, showing isometric unit cell (a) and an arrangement of the isometric and a fully twisted elementary cell (b).

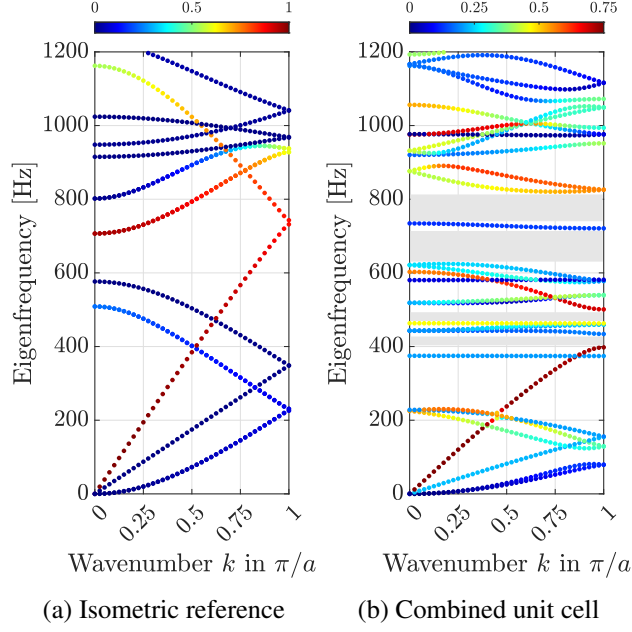(a) Isometric reference   (b) Combined unit cell

Figure 14: Dispersion relation in the irreducible BRILLOUIN zone for the isometric (a) and combined (b) unit cell as shown in Fig. 13. Colors indicate the polarization of modes from in-plane (blue) to out-of-plane (red). Grey regions highlight full band gaps.

the isometric with the fully twisted arrangement, the unit cell's effective stiffness decreases significantly, leading to collective downward shifts of dispersion bands and therefore, an increased density of modes in the observed frequency range. Seemingly, the axial stiffness is affected considerably as the first longitudinal out-of-plane branch approaches the edge of the BRILLOUIN zone at only $398\,\mathrm{Hz}$ and exhibits a frequency gap of $100\,\mathrm{Hz}$ to the optical branch, whereas the acoustical and optical branch of torsion are not disrupted as observed in Sec. 3.3. The polarization factor of both out-of-plane branches does not exceed a level of $p = 0.75$, unlike the isometric unit cells, which approach $p = 1$ for longitudinal wave motion. This difference stems from axial-rotation motion coupling in all faces of the chiral elementary cell, which affects corresponding mode shapes. As the unit cell expands, twisted faces rotate and extend in-plane, thus inducing in-plane deformations despite the wave's overall out-of-plane polarization. Vice versa, the polarization of in-plane torsional branches increases to values of $p = 0.23$ compared to $p \approx 0$ for the isometric design, governed by a compression-extension movement of the twisted block as the cells rotate with respect to the $z-$axis. Despite these indications of a coupling effect, a partial gap between the longitudinal and torsional branches as observed in the previous studies is not present. Furthermore, the dispersion relation of the combined

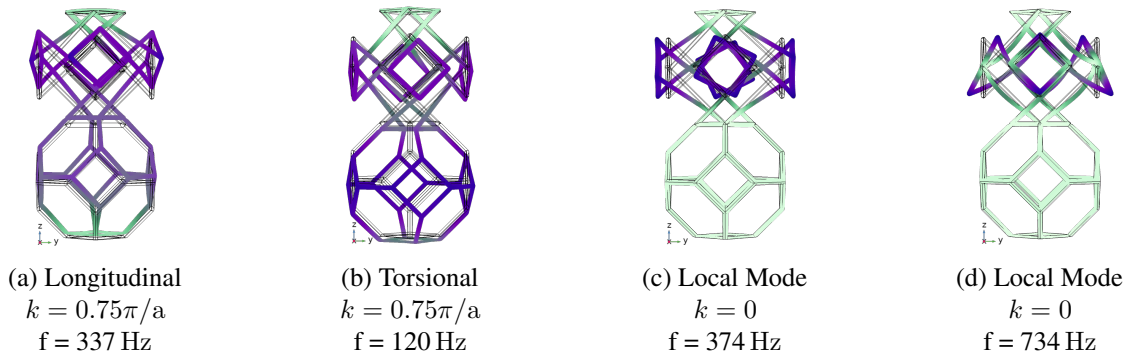| (a) Longitudinal | (b) Torsional | (c) Local Mode | (d) Local Mode |
| $k = 0.75\pi/a$ | $k = 0.75\pi/a$ | $k = 0$ | $k = 0$ |
| f = 337 Hz | f = 120 Hz | f = 374 Hz | f = 734 Hz |

Figure 15: Mode shapes of the combined unit cell. (a) and (b) demonstrate compression-torsion coupling in waves of both polarizations, (c) and (d) local vibrations of twisted faces, corresponding to flat bands in the dispersion relation (compare Fig. 14b).

arrangement is populated by flat bands in both lower and higher-frequent regimes, i.e. visible at $374\,\mathrm{Hz}$ and $734\,\mathrm{Hz}$. The corresponding mode shapes are characterized by local vibrations of the twisted square faces, while the remaining structure hardly deforms. Fig. 15 gives an example of such mode shapes. Emerging flat bands and the corresponding close-to-zero group speed indicate that these modes are not propagative and remain localized. Therefore, the structure supports a wide band gap in the range of $624\,\mathrm{Hz}$ to $820\,\mathrm{Hz}$, which is absent in the dispersion relation of the isometric design.

As a result, combinations of the stiff isometric reference cell and cells that are softened from multi-axial twists could provide a way to design lattice arrangements with significant band gap performance in the low-frequent regime while recovering a portion of the isometric cell's stiffness. Coupled modes of twisted cells may be further exploited to generate a coupled translational-rotational resonator with square faces serving as a host for mass inclusions that might amplify the rotational inertial properties.

4 Conclusion

In this contribution, a design approach for periodic lattice materials is presented. Starting from the isometric Kelvin cell as a fundamental building block, a twisting approach is formulated, which imposes rigid body rotations on the cell's square faces while retaining the truss connection pattern to generate three-dimensional cellular architectures. By constraining opposing square faces with counterclockwise rotations, chirality within the cell is attainable. As a key feature, twisted cells are topologically equivalent to the isometric Kelvin cell, and the simple-cubic lattice characteristic is maintained.

In a comparative study, the dispersion relation of 1D infinite structures formed by unit cells with altering twist properties is analyzed. The results outline that the wave dispersion characteristics can be considerably varied depending on the rotation angle and the chosen set of twisted faces. In particular, twisting the Kelvin cell is accompanied by inherent changes in the unit cell's effective stiffness characteristics. As the frequency shift of modes due to varying stiffness depends on their polarization, the relative spacing between dispersion bands can be altered as a function of the twist angle, giving rise to full band gaps, which are absent in the isometric Kelvin cell. By suitably varying the stiffness characteristics as a consequence of twisting, it is possible to design lattice architectures whose dispersive properties are similar to monoatomic and diatomic mass-spring systems. In the latter case, significant band gaps in the low-frequent regime are attainable, and band gap tunability as a function of the twist angle is demonstrated.

Particular focus is directed to the effects of twisting-induced chirality. By analyzing the mode shapes and quantifying their polarization, significant indications of compression-torsion coupled wave motions can be found in chiral structures, which are driven by axial-rotary motions of twisted square faces. In selected unit cell configurations, this enforces partial frequency gaps at the crossing points of longitudinal and torsional branches. In case twisting is applied to all square faces at large rotation angles, flat bands emerge in the spectrum, induced by highly-localized modes as vibrations are encapsulated within twisted faces.

The results highlight the potential of twisted Kelvin cells to provide building blocks for lattice materials with band gap properties and tunable performance. Unit now, full tunability is not achieved as the relation between twisting, cell stiffness, and the corresponding frequency shift of dispersion bands having different polarization has not been established. Furthermore, one should be aware that this preliminary study solely focuses on dynamic properties and neglects the potential consequences of twisting for the static-elastic properties, which are likewise essential for the performance of lattice-based structures. Yet, the Kelvin cell design approach could provide another step towards multi-functional lattices with tailorable properties on the macro-scale. As twisting is applicable independently in three principal axis directions, modular design of Kelvin cell-based units is enabled, with the prospect to realize spatially varying properties such as heterogeneous stiffness. In connection with a high accessibility to additive manufacturing techniques, this makes the Kelvin cell approach an interesting candidate for other functionalities such as damping or energy absorption performances.

References

[1] S. A. Cummer, J. Christensen, and A. Alù, "Controlling sound with acoustic metamaterials," *Nature Reviews Materials*, vol. 1, no. 3, p. 2059, 2016.

[2] M. Kadic, G. W. Milton, M. van Hecke, and M. Wegener, "3d metamaterials," *Nature Reviews Physics*, vol. 1, no. 3, pp. 198–210, 2019.

[3] T. A. Schaedler and W. B. Carter, "Architected cellular materials," *Annual Review of Materials Research*, vol. 46, no. 1, pp. 187–210, 2016.

[4] T. Bückmann, M. Thiel, M. Kadic, R. Schittny, and M. Wegener, "An elasto-mechanical unfeelability cloak made of pentamode metamaterials," *Nature communications*, vol. 5, p. 4130, 2014.

[5] Z. Wang, C. Luan, G. Liao, J. Liu, X. Yao, and J. Fu, "Progress in auxetic mechanical metamaterials: Structures, characteristics, manufacturing methods, and applications," *Advanced Engineering Materials*, vol. 22, no. 10, p. 2000312, 2020.

[6] C. C. Claeys, K. Vergote, P. Sas, and W. Desmet, "On the potential of tuned resonators to obtain low-frequency vibrational stop bands in periodic panels," *Journal of Sound and Vibration*, vol. 332, no. 6, pp. 1418–1436, 2013.

[7] C. Claeys, E. Deckers, B. Pluymers, and W. Desmet, "A lightweight vibro-acoustic metamaterial demonstrator: Numerical and experimental investigation," *Mechanical Systems and Signal Processing*, vol. 70-71, no. 8, pp. 853–880, 2016.

[8] T. Delpero, S. Schoenwald, A. Zemp, and A. Bergamini, "Structural engineering of three-dimensional phononic crystals," *Journal of Sound and Vibration*, vol. 363, no. 1, pp. 156–165, 2016.

[9] L. Liu and M. I. Hussein, "Wave motion in periodic flexural beams and characterization of the transition between bragg scattering and local resonance," *Journal of Applied Mechanics*, vol. 79, no. 1, 2012.

[10] L. D'Alessandro, R. Ardito, F. Braghin, and A. Corigliano, "Low frequency 3d ultra-wide vibration attenuation via elastic metamaterial," *Scientific reports*, vol. 9, no. 1, p. 8039, 2019.

[11] S. Krödel, T. Delpero, A. Bergamini, P. Ermanni, and D. M. Kochmann, "3d auxetic microlattices with independently controllable acoustic band gaps and quasi-static elastic moduli," *Advanced Engineering Materials*, vol. 16, no. 4, pp. 357–363, 2014.

[12] L. Junyi and D. S. Balint, "A parametric study of the mechanical and dispersion properties of cubic lattice structures," *International Journal of Solids and Structures*, vol. 91, no. 1838, pp. 55–71, 2016.

[13] Y. Liu, X.-z. Sun, W.-z. Jiang, and Y. Gu, "Tuning of bandgap structures in three-dimensional kagome-sphere lattice," *Journal of Vibration and Acoustics*, vol. 136, no. 2, p. 2022, 2014.

[14] E. Baravelli and M. Ruzzene, "Internally resonating lattices for bandgap generation and low-frequency vibration control," *Journal of Sound and Vibration*, vol. 332, no. 25, pp. 6562–6579, 2013.

[15] X. An, H. Fan, and C. Zhang, "Elastic wave and vibration bandgaps in planar square metamaterial-based lattice structures," *Journal of Sound and Vibration*, vol. 475, p. 115292, 2020.

[16] W. Thomson, Baron Kelvin, *Baltimore Lectures on Molecular Dynamics and the Wave Theory of Light*, ser. Cambridge Library Collection - Physical Sciences. Cambridge University Press, 2010.

[17] A. H. Orta and C. Yilmaz, "Inertial amplification induced phononic band gaps generated by a compliant axial to rotary motion conversion mechanism," *Journal of Sound and Vibration*, vol. 439, no. 09, pp. 329–343, 2019.

[18] C. Yilmaz, G. M. Hulbert, and N. Kikuchi, "Phononic band gaps induced by inertial amplification in periodic media," *Physical Review B*, vol. 76, no. 5, 2007.

[19] A. Bergamini, M. Miniaci, T. Delpero, D. Tallarico, B. van Damme, G. Hannema, I. Leibacher, and A. Zemp, "Tacticity in chiral phononic crystals," *Nature communications*, vol. 10, no. 1, p. 4525, 2019.

[20] Y. Mi and X. Yu, "Sound transmission of acoustic metamaterial beams with periodic inertial amplification mechanisms," *Journal of Sound and Vibration*, vol. 499, p. 116009, 2021.

[21] X. N. Liu, G. K. Hu, C. T. Sun, and G. L. Huang, "Wave propagation characterization and design of two-dimensional elastic chiral metacomposite," *Journal of Sound and Vibration*, vol. 330, no. 11, pp. 2536–2553, 2011.

[22] X. Fei, L. Jin, X. Zhang, X. Li, and M. Lu, "Three-dimensional anti-chiral auxetic metamaterial with tunable phononic bandgap," *Applied Physics Letters*, vol. 116, no. 2, p. 021902, 2020.

[23] Y. Chen, T. Frenzel, S. Guenneau, M. Kadic, and M. Wegener, "Mapping acoustical activity in 3d chiral mechanical metamaterials onto micropolar continuum elasticity," *Journal of the Mechanics and Physics of Solids*, vol. 137, p. 103877, 2020.

[24] W. Xu, Z. Liu, L. Wang, and P. Zhu, "3d chiral metamaterial modular design with highly-tunable tension-twisting properties," *Materials Today Communications*, vol. 30, p. 103006, 2022.

[25] H. Mao, R. Rumpler, M. Gaborit, P. Göransson, J. Kennedy, D. O'Connor, D. Trimble, and H. Rice, "Twist, tilt and stretch: From isometric kelvin cells to anisotropic cellular materials," *Materials & Design*, vol. 193, p. 108855, 2020.

[26] H. Mao, R. Rumpler, and P. Göransson, "An inverse method for characterisation of the static elastic hooke's tensors of solid frame of anisotropic open-cell materials," *International Journal of Engineering Science*, vol. 147, no. 1–2, p. 103198, 2020.

[27] M. Miniaci, A. S. Gliozzi, B. Morvan, A. Krushynska, F. Bosia, M. Scalerandi, and N. M. Pugno, "Proof of concept for an ultrasensitive technique to detect and localize sources of elastic nonlinearity using phononic crystals," *Physical review letters*, vol. 118, no. 21, p. 214301, 2017.

[28] S. Krödel, A. Palermo, and C. Daraio, "Acoustic properties of porous microlattices from effective medium to scattering dominated regimes," *The Journal of the Acoustical Society of America*, vol. 144, no. 1, p. 319, 2018.

[29] N. Jiménez, O. Umnova, and J.-P. Groby, *Acoustic Waves in Periodic Structures, Metamaterials, and Porous Media*. Cham: Springer International Publishing, 2021, vol. 143.

[30] F. Farzbod and O. E. Scott-Emuakpor, "Interactions beyond nearest neighbors in a periodic structure: Force analysis," *International Journal of Solids and Structures*, vol. 199, pp. 203–211, 2020.

[31] Y. Chen, M. Kadic, and M. Wegener, "Roton-like acoustical dispersion relations in 3d metamaterials," *Nature communications*, vol. 12, no. 1, p. 3278, 2021.